Twenty Years of Polar Winds from AVHRR: Validation and Comparison with ERA-40

RICHARD DWORAK

Cooperative Institute for Meteorological Satellite Studies, University of Wisconsin—Madison, Madison, Wisconsin

JEFFREY R. KEY

NOAA/NESDIS Center for Satellite Applications and Research, Madison, Wisconsin

(Manuscript received 30 August 2007, in final form 27 May 2008)

ABSTRACT

Recent studies have shown that the Arctic climate has changed markedly over the past 20 years. Two major reanalysis products that can be used for studying recent changes unfortunately exhibit relatively large errors in the wind field over the Arctic where there are few radiosonde data available for assimilation. At least 10 numerical weather prediction centers worldwide have demonstrated that satellite-derived polar winds have a positive impact on global weather forecasts. The impact on reanalyses should be similar. Therefore, a polar wind dataset spanning more than 20 years was generated using Advanced Very High Resolution Radiometer (AVHRR) data. Comparisons with winds from radiosondes show biases in the AVHRR-derived winds of 0.1–0.8 m s^{-1}, depending on the level. In addition, AVHRR has lower root-mean-square speed errors and speed biases than the 40-yr ECMWF reanalysis product (ERA-40) when compared with rawinsondes not assimilated into the reanalysis. Therefore, it is recommended that the historical AVHRR polar winds be assimilated into future versions of the reanalysis products. The authors also explore possible kinematic reasons for the disparities between ERA-40 and AVHRR wind fields. AVHRR and ERA-40 speed and direction differences for various kinematic flow features are investigated. Results show that, on average, AVHRR winds are faster in jet streams and ridges but are slower in troughs and jet exit regions. The results from this study could lead to a better dynamical understanding of why the reanalysis product produces a less-accurate wind vector field over regions that are void of radiosonde data.

1. Introduction

Numerous studies have reported on recent changes in climate over the Arctic and parts of the Antarctic (Serreze et al. 2000; Turner et al. 2006; Wang and Key 2005b; Comiso 2003; Polyakov et al. 2003). Observations over the past few decades indicate that temperatures over the Arctic and parts of the Antarctic have risen significantly (Wang and Key 2005b; Comiso 2003; Turner et al. 2006) and that cyclonic activity over the Arctic and seas near the Antarctic has also increased (Zhang et al. 2004; Fyfe 2003; Key and Chan 1999). Furthermore, there has been a dramatic decrease in sea ice coverage over the Arctic and Amundsen–Bellinghausen Seas of the Antarctic (Comiso 2002; Lindsay and Zhang 2005; Jacobs and Comiso 1997; Turner et al. 2006) and changes in atmospheric circulation patterns over the Arctic and Antarctic, with shifts in the Arctic Oscillation and Antarctic Oscillation to a more positive phase (Holland 2003; Thompson and Solomon 2002; Turner et al. 2006).

An important tool for diagnosing climate changes over the polar regions is an atmospheric reanalysis, such as the National Centers for Environmental Prediction–National Center for Atmospheric Research (NCEP–NCAR) and European Centre for Medium-Range Weather Forecasts (ECMWF) reanalysis products. These data have been shown to have reasonably accurate temperature fields (Uppala et al. 2005). However, it has also been shown that the reanalyses have relatively large errors in their wind fields over the Arctic (Francis 2002), likely as a result of the paucity of wind observations for assimilation over the Arctic (Fig.

Corresponding author address: Richard Dworak, Cooperative Institute for Meteorological Satellite Studies, University of Wisconsin—Madison, 1225 West Dayton St., Madison, WI 53706.
E-mail: rdworak@ssec.wisc.edu

DOI: 10.1175/2008JAMC1863.1

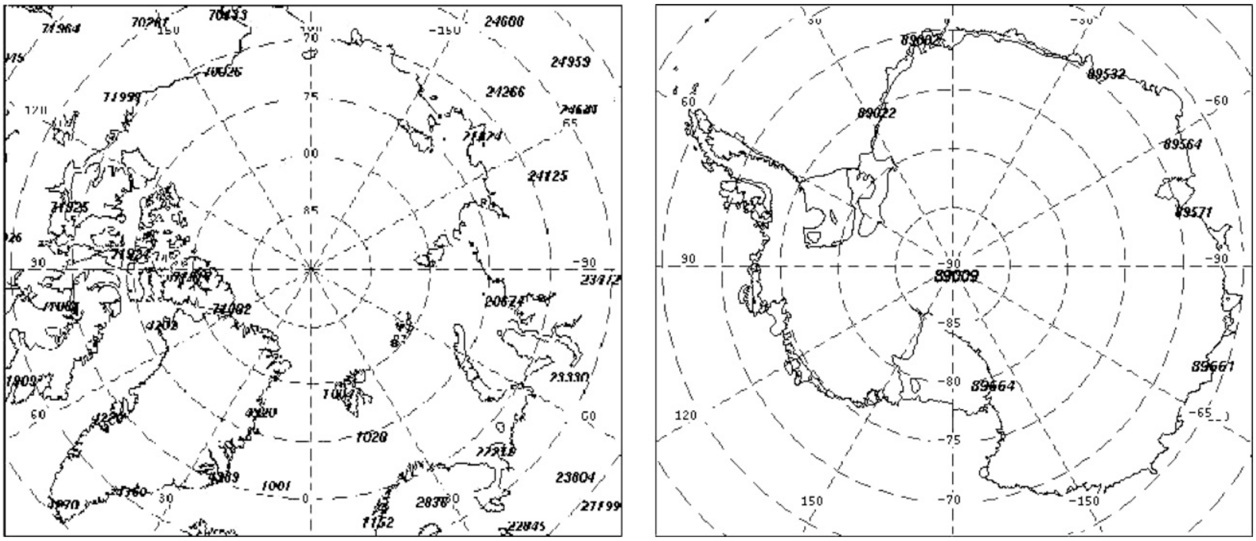

FIG. 1. Rawinsonde observing network over the (left) Arctic and (right) Antarctic.

1). Francis (2002) examined differences between NCEP–NCAR and ECMWF reanalysis winds and radiosonde winds (or rawinsondes, hereinafter raob) that were not assimilated in the reanalysis field, using data from the Arctic Leads Experiment (LeadEx) from 1992 and the Coordinated Eastern Arctic Experiment (CEAREX) from 1988 and 1989. It was found that both reanalyses exhibit large biases in the zonal and meridional wind components, being too westerly and too northerly by 25%–65%. Overly strong westerlies suggest that the magnitudes of the meridional temperature gradients near the experiment sites are too high (Francis et al. 2005). The reanalysis fields could therefore have overly intense, narrow jet streams and/or cyclonic disturbances, semipermanent features in the upper-level circulation may be misplaced, and the reanalysis may not properly capture the synoptic-scale feature that tends to cause these fluctuations (Francis et al. 2005). Important is that poleward transport of energy and moisture by the reanalysis winds would be too small. Therefore, there needs to be a way to improve the wind fields over the polar regions by providing more wind observations.

An attempt to improve the three-dimensional wind fields for climate reanalyses has been undertaken by Francis et al. (2005) using satellite-derived temperature profiles from the Television and Infrared Observation Satellite Operational Vertical Sounder (TOVS) and the thermal-wind relationship. The methods and mass conservation technique used in producing the satellite-derived winds from TOVS temperature soundings are explained further in Zou and Van Woert (2002) and Francis et al. (2005). However, Greenland itself acts as a mass barrier below 700 hPa that probably had an unfortunate and important negative impact on the mass conservation technique (Zou and Van Woert 2002) used for the zonal direction at lower levels (Francis et al. 2005). In addition, in using the thermal-wind relationship, the resultant wind field would be nearly geostrophic and would not take into account any significant ageostrophic motions in the flow (Zou and Van Woert 2001). In the real atmosphere, flows are ageostrophic under certain conditions (friction, accelerations, and decelerations of the flow), and therefore the thermal-wind product would be less accurate in regions of significant ageostrophic flow, such as in the entrance and exit regions of jet streaks and in strongly curved flows, because the geostrophic balance only occurs when there is no curvature in the flow (Holmlund 1998).

Another source of error in the geostrophic approximation stems from neglecting the acceleration terms (dv/dt and du/dt) in horizontal momentum equations:

$$dv/dt = -f_0 u - 1/\rho(\partial P/\partial y) \quad \text{and} \tag{1a}$$

$$du/dt = f_0 v - 1/\rho(\partial P/\partial x), \tag{1b}$$

where t is time, x and y are Cartesian coordinates, P is pressure, ρ is density, u (v) is the east–west (north–south) component of the wind vector, and f_0 is the Coriolis parameter. This becomes a major factor in regions in which the flow rapidly accelerates or decelerates, for example, in the entrance and exit regions of jet streams, or in curved flows with significant centripetal acceleration such as the base of a trough of low pressure. For example, in one case study done on 2 March 1979 off the coast of Baja California, it was found that the speed of the 300-hPa cross-height contour ageostrophic wind component in the left exit region of a jet streak in a highly curved flow around the back end of an amplified upper-level trough of low pressure exceeded 20 m s^{-1} (Shapiro and Kennedy 1981). Moreover, the observed inaccuracies of the reanalysis wind fields are expected to occur in regions of ageostrophic flow, and the satellite-derived thermal-wind field would not improve the reanalysis deficiencies in those regions because the thermal winds are nearly geostrophic.

Satellite imagers can be used to estimate the true wind. Clouds and water vapor features are tracked in sequential images under the assumption that their movement represents the local airflow, be it geostrophic or ageostrophic. With a gap in the observing systems over the polar regions that cannot be filled by geostationary satellites because of poor viewing geometries, polar-orbiting satellites are needed. Because winds derived from polar-orbiting satellite imagers have been used to improve weather forecasts (Key et al. 2003; Velden et al. 2005), they could also be used to improve the reanalysis wind fields. For long-term reanalyses, the Advanced Very High Resolution Radiometer (AVHRR) that is on National Oceanic and Atmospheric Administration (NOAA) satellites would be suitable because of its relatively long record going back to the early 1980s. Therefore, a dataset of AVHRR wind vectors over the polar regions was created, spanning more than 20 years (January 1982–August 2002). Unlike the Moderate Resolution Imaging Spectroradiometer (MODIS) on the National Aeronautics and Space Administration (NASA) *Terra* and *Aqua* satellites, AVHRR does not have a water vapor channel and therefore produces fewer wind vectors at middle and upper levels over the Arctic and the Antarctic. Wind vectors are estimated for the Arctic and Antarctic, poleward of approximately 60° latitude, by tracking the movement of cloud features in the 11-μm window channel. In this paper, the historical AVHRR polar wind product is described. The satellite-derived atmospheric motion vectors (AMV) are compared with winds from radiosondes and with the 40-yr ECMWF reanalysis (ERA-40) winds for different flow types. An analysis of AVHRR and ERA-40 speed and direction differences for kinematic flow features is performed. The potential impacts of assimilating AVHRR winds into reanalyses are also discussed.

2. Data

AVHRR global area coverage (GAC) data, ERA-40, the Integrated Global Radiosonde Archive (IGRA), and rawinsonde observations from LeadEx and CEAREX are used in this study.

TABLE 1. Letter code, satellite number, identifier (ID), and dates of operational use of the NOAA satellites with the AVHRR instrument aboard.

Code	Satellite No.	ID	Operational dates
TN	5	1	11 Jun 1978–1 Nov 1980
A	6	3	17 Jul 1979–9 Jul 1986
C	7	7	24 Jun 1981–7 Oct 1985
E	8	13	24 Jun 1981–8 Jan 1985
F	9	11	17 Dec 1984–19 Jan 1995
G	10	15	8 Oct 1986–6 Oct 1994
H	11	1	21 Oct 1988–15 Sep 1994
D	12	9	16 Jul 1991
J	14	5	19 Jan 1995
K	15	7	13 May 1998–10 Jul 2000
L	16	3	21 Sep 2000
M	17	11	24 Jun 2002
N	18	13	20 May 2005

a. AVHRR

The AVHRR imager on the NOAA polar-orbiting satellites makes 14 orbits per day over the Arctic and Antarctic, with an orbital period of about 100 min. AVHRR has six channels that include one visible (0.6 μm), one near-infrared (IR, 0.9 μm), one reflected IR (3.7 μm), and two thermal IR (11 and 12 μm) channels. The entire AVHRR dataset covers the years 1978 (*NOAA-5*) through the time of writing (*NOAA-18*) and is summarized in Table 1. The 11-μm window channel radiances are used in the AVHRR historical winds dataset, which covers the period from 1 January 1982 to 31 August 2002. Even though AVHRR has a visible channel, it is not generally useful for winds in polar regions because of the long winter darkness and low sun angles during the summer that make feature tracking difficult. With monthly average cloud amounts over the Arctic and Antarctic ranging from 50% to 90% and an annual mean cloud coverage of about 70% over the Arctic (Wang and Key 2005a), potential cloud targets are numerous (Key et al. 2003). Overlap between successive orbits is relatively high in the polar regions, and therefore winds are generally estimated poleward of about 70° latitude.

For satellite data to be used in long-term studies, as would be the case if the winds were assimilated in a reanalysis system, differences among satellites in the time series (e.g., *NOAA-7*, *-9*, and *-11*) must be considered. Calibration differences and changes in equator crossing time can produce biases. However, these issues do not significantly affect the historical wind product for two reasons. First and foremost, the feature tracking depends only on consistency from one orbit to the next. Second, although satellite drift will result in changes in temporal sampling throughout the day at any given location, the exact observation times are known and can be used by assimilation systems.

b. ERA-40

The ERA-40 is a reanalysis of meteorological observations from September 1957 to August 2002 that was produced by ECMWF (Uppala et al. 2005). The data assimilation uses analysis steps that are usually 6 h and combines observations over the period with background information to produce an estimate of the state of the atmosphere at a specific time (Uppala et al. 2005). The background information used in the reanalysis that was required for each analysis time is a short-term forecast out to 9 h ahead of the initialization (Uppala et al. 2005). The background forecasts and observations are combined by statistically minimizing their errors in a 3D variational assimilation scheme (Uppala et al. 2005).

Upper-air wind observations in ERA-40 come from radiosondes, dropsondes, pilot balloons, profilers, aircraft, and tracking features (cloud and water vapor) from geostationary satellites (Uppala et al. 2005). However, there are no geostationary satellite–derived winds over the polar regions, and winds from low earth-orbiting satellites are not assimilated. The accuracy of radiosonde observations improved over the period; however, the geographical and temporal coverage has declined since 1979 (Uppala et al. 2005). To compensate for the decline of radiosonde observations, there has been an increase in the use of satellite observations (Uppala et al. 2005), such as AMVs from geostationary satellites and radiances from infrared and passive microwave atmospheric sounders.

Successful modeling of the evolving state of the atmosphere depends on the utilization of observations, dynamics, and physics of the background forecast model or any dynamical or physical relationships built into the error statistics (Uppala et al. 2005). The degree of dependence on the model varies with density and relative accuracy of the observations and, in general, can vary from place to place and from one variable to another (Uppala et al. 2005). Deficiencies in model physics, background information, or observation error statistics; interactions between the forecast background and observations in the assimilation; and bad observations can lead to the biases observed by Francis (2002) in the ERA-40 Arctic winds.

c. IGRA

The radiosonde winds used for validation come from the IGRA. The IGRA dataset is quality controlled, with assurances that the wind vectors have plausible values of wind speed (0–150 m s^{-1}) and direction (0°–360°) without vertical value repetition runs and that the dates and times of the observations are correct (Dure et al. 2006). It has been noted that radiosonde wind speeds are of good quality, with total radiosonde error between about 0.9 m s^{-1} at 900 hPa and about 2.1 m s^{-1} at 100 hPa, (Kitchen 1989) and that mean directional differences are about 1° (Schmetz et al. 1993). However, beyond a distance separation of 52 km from the observation the vector root-mean-square (RMS) difference is about 2.5 m s^{-1} at 850 hPa and 4 m s^{-1} at 300 hPa, and at a time separation of 2 h from the observation the vector RMS difference is about 2.2 m s^{-1} at 850 hPa and 5.1 m s^{-1} at 300 hPa (Kitchen 1989).

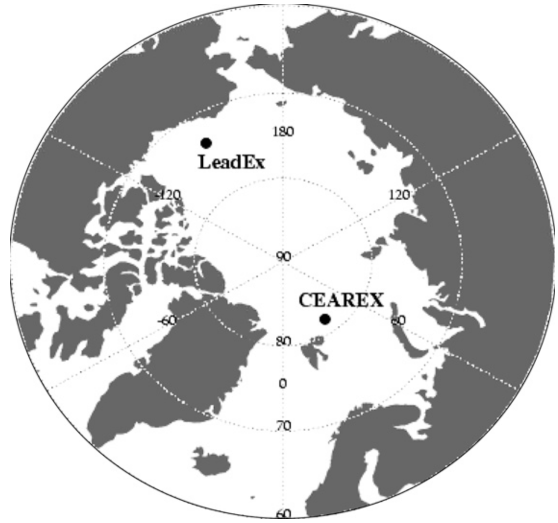

FIG. 2. Locations of the LeadEX and CEAREX sites (from Francis 2002).

d. LeadEx and CEAREX

CEAREX was a multinational field project that occurred northeast of Spitsbergen, Norway, off the coast of Svalbaard from September 1988 to May 1989. During the project, meteorological (including rawinsonde) data were collected on a multiplatform ship *Polarbjorn* as it drifted southward from within the pack ice, east of Svalbard, and ultimately into open water (Francis 2002). LeadEx was a field experiment that occurred in the Beaufort Sea on the pack ice approximately 270 km north of Prudhoe Bay, Alaska (Francis 2002). During LeadEx, rawinsondes were launched from 19 March to 22 April 1992. CEAREX and LeadEx (Fig. 2) combine to provide 9 months of rawinsonde data that are used for validation of AVHRR winds versus ERA-40. Winds from both experiments were measured using omega tracking, with accuracies of approximately 4 m s^{-1} for a single wind value (Francis 2002).

3. Methods

The cloud motion vector method used for AVHRR originated from Turner and Warren (1989) and is very similar to the methods used for MODIS IR and Geostationary Operational Environmental Satellite winds that are described in depth by Nieman et al. (1997).

a. Wind estimation

Before winds are derived from the satellite imagery, AVHRR GAC channel-4 data are calibrated and navigated to a polar stereographic projection with a 4-km pixel size. A triplet of images composed of three successive orbits is used. ERA-40 climate reanalysis fields are used as the background in the wind estimation. The ERA-40 data are interpolated from the standard 2.5° latitude/longitude format to a 1° format, and the two closest analysis times (within 6 h of each other) are interpolated to the time of the center image in the triplet.

The first step in wind derivation is targeting. Local gradients around a single pixel with the lowest brightness temperature in a search box are calculated to determine if there are potential targets for tracking. To determine the heights of the targets, the infrared window channel method is used. This method compares the IR window channel brightness temperature with the temperature profiles given by the background analysis field. Cloud heights are determined by interpolating the cloud temperature, which is an average value over a set number of pixels, to the interpolated analysis background field temperatures.

Next, subsequent images are searched for the targets. This is done by a statistical analysis of the search boxes, determining the highest correlated point between the initial target location and the ensuing search box region. These steps are repeated for images 2 and 3 in the triplet to produce another vector. The two vectors are compared with each other and with the background field to determine the initial quality of vectors. If the two vectors are sufficiently similar, the initial wind vector is an average of the two with the time of the middle image. Acceleration checks are performed to determine the physical validity of the wind vector.

In the postprocessing steps, quality indicators (QI) are computed (Holmlund et al. 2001). The quality indicators are primarily for the end users to determine observational weights and error characteristics of the satellited-derived winds being assimilated. A sample of the AVHRR winds over a 9-day period is given in Fig. 3.

b. Validation

In the validation of the AVHRR winds, the RMS difference and normalized RMS (NRMS) are used:

$$\mathrm{RMS} = \left[\frac{\sum(s_{\mathrm{sat}} - s_{\mathrm{raob}})^2}{n}\right]^{1/2}, \qquad (2)$$

where s_{sat} is the satellite-derived wind speed, s_{raob} is the rawinsonde wind speed, and n is the number of cases. NRMS is the RMS divided by the rawinsonde wind speed. It has been shown that the RMS difference of the cloud-drift winds decreases monotonically with an increase in the recursive-filter QI (Hayden and Purser 1995). Similar results were found with QIs when compared with values for high-level IR cloud-drift winds (Holmlund 1998). However, the results were poorer for mid- and low-level IR winds, with a nonmonotonic increase (decrease) of QI with a decrease (increase) of NRMS (Holmlund 1998).

Validation was done by comparing the AVHRR winds with rawinsondes to determine how close the AVHRR winds are to actual observations, assuming that winds from raobs represent the actual wind. The AVHRR and ERA-40 winds are also compared with rawinsonde observations that are not assimilated in the reanalysis, providing an assessment of how the AVHRR and ERA-40 winds compare to one another and giving final validation on whether AVHRR outperforms ERA-40 in regions that are void of wind data.

c. Potential sources of error

Wind vector derivation is a complex process, and there are potential sources of error that could have adverse effects on target selection, tracking, and height determination. Even though there are postprocessing procedures that attempt to flag wind vectors with errors, it is not guaranteed that all the erroneous wind vectors will be eliminated. One potential source of error is parallax. The parallax problem is an orbital issue that causes the targets being tracked off nadir to be viewed by the satellite as being displaced farther than they are in actuality. The farther the target being tracked is from nadir and from the earth's surface, the larger the apparent displacement. For example, at 500 km from nadir the apparent location of a cloud with a height of 3 km will be approximately 2.1 km farther from nadir than its actual position. However, testing with MODIS winds indicates that parallax is not a significant problem because the area of overlap in the images of a triplet, which is where winds can be derived, does not include regions of extreme viewing geometry.

The infrared window method used for cloud height

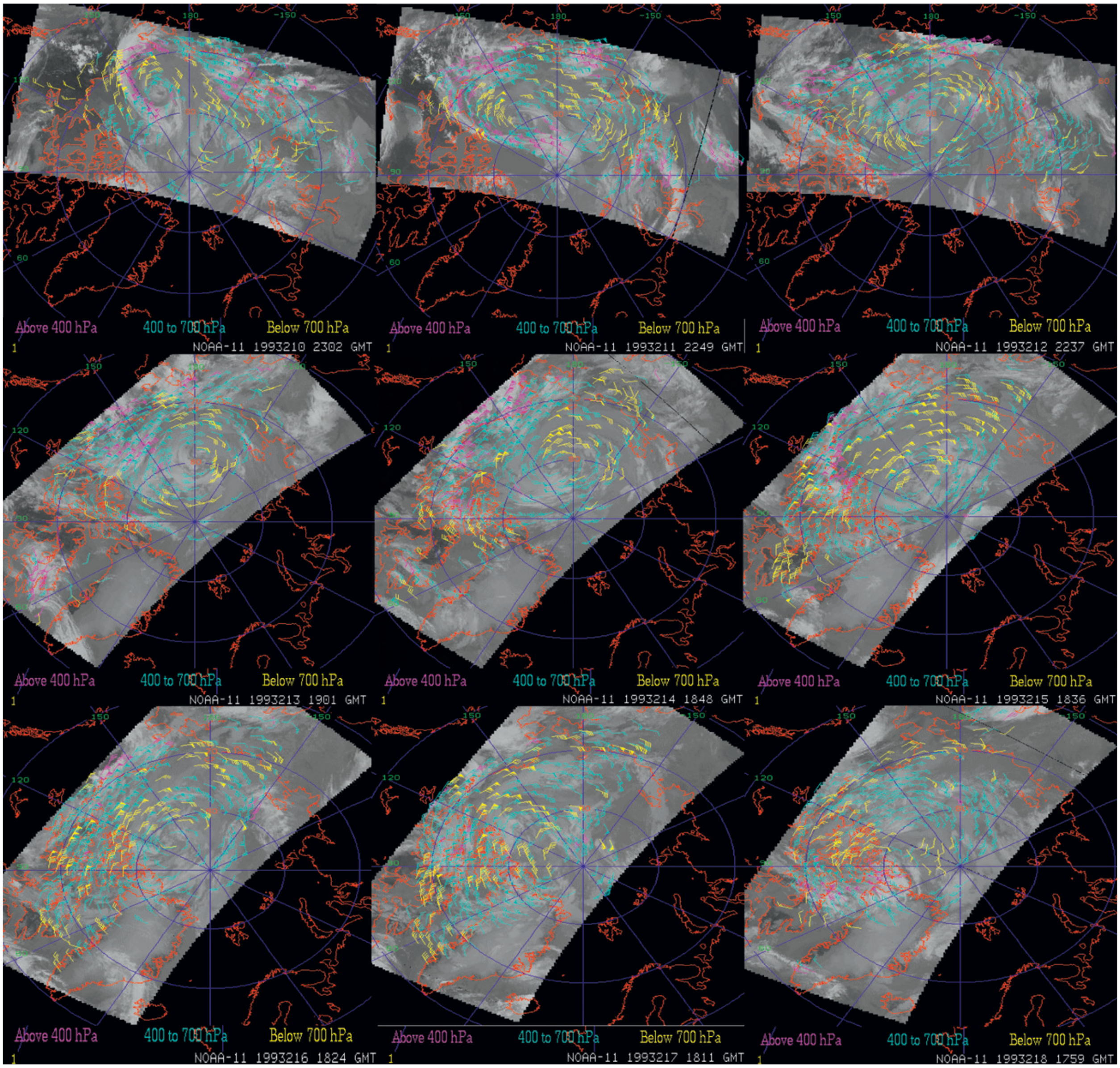

FIG. 3. A 9-day sample of AVHRR winds over the Arctic. The *NOAA-11* AVHRR images and derived winds show the progression of a cyclone over the western Arctic Ocean.

assignment in the AVHRR winds processing is good at determining heights for opaque clouds but has been shown to be inaccurate for thin cirrus clouds. In such cases, the surface contributes significantly to the upwelling radiance, resulting in brightness temperatures that are too high and cloud heights that are too low (Fig. 4) (Holmlund 1998; Key et al. 2003). Another source of error in the height determination is the location of the top of the boundary layer, which is a spatially (in the vertical direction) small feature that can be easily misplaced in the background field and can lead to incorrect height assignments of low-level winds (Holmlund 1998). Furthermore, potential problems with height assignments of low-level wind vectors arise from the temperature structure of the Arctic and Antarctic atmospheres, especially with respect to the location of temperature inversions. The atmospheric temperature structure of the Arctic or Antarctic has ubiquitous temperature inversions and isothermal layers (Liu and Key 2003; Liu et al. 2006) that make height assignments difficult.

There are other height assignment techniques that are better under certain circumstances, such as the carbon dioxide (CO_2)-infrared window ratio or the water

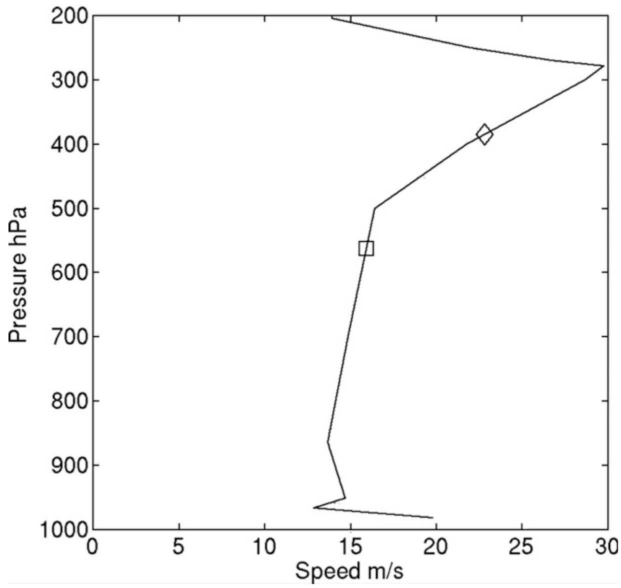

FIG. 4. A sounding of the U component of wind speed over Ostrov Dikson, Russia, at 0000 UTC 5 Aug 1992. The AVHRR wind observation collocated in space and time was 23.10 m s^{-1} and 263°. The box is the assigned pressure height for the AVHRR wind observation, and the diamond is the best-fit height assignment based on the AVHRR U-component wind observation in comparison with the radiosonde profile of U component of wind speed.

vapor (H_2O)-infrared window intercept methods. However, because of the limitation of the AVHRR in having no CO_2 or H_2O channels, the infrared window method is the only viable method. With the IR window method having potential issues in height assignment of wind vectors, are the AVHRR wind retrievals accurate enough to be included in reanalysis products?

4. Validation

The traditional approach to determining the quality of satellite-derived winds is to compare them with observed winds from radiosondes (Holmlund 1998; Holmlund et al. 2001; Nieman et al. 1997; Velden et al. 1997). In addition, we compare the AVHRR and ERA-40 winds with rawinsonde observations that are not assimilated in ERA-40, providing an assessment of how the AVHRR and ERA-40 winds compare to one another and how well the ERA-40 winds are in regions that are void of wind data. Validation statistics for AVHRR winds relative to radiosonde winds from IGRA, observations that are for the most part assimilated into the reanalyses of ERA-40 and NCEP–NCAR (Haimberger 2005), are given in Table 2. The comparisons cover the area north of 60° latitude over the periods from 1 August 1988 to 21 May 1989 and from 8 March to 22 July 1992. Only collocations with the radiosonde and AVHRR wind vector within a radius of 100 km in the horizontal plane, 50 hPa in the vertical direction, and 1 h in time are used.

TABLE 2. AVHRR wind statistics when compared with raob winds over the Arctic.

	Low level (<700 hPa)	Midlevels (700–400 hPa)	Upper levels (>400 hPa)
Speed RMS (m s^{-1})	4.98	5.18	7.57
Speed bias (m s^{-1})	+0.1	−0.29	+0.77
Avg speed diff (m s^{-1})	3.64	3.81	5.40
Direction RMS (°)	65.17	52.55	42.40
Direction bias (°)	−0.49	−0.71	+1.48
Avg direction diff (°)	46.1	34.01	25.07
Mean AVHRR speed (m s^{-1})	7.42	11.17	21.04
Mean raob speed (m s^{-1})	7.32	11.46	20.28
NRMS	0.68	0.45	0.37
Correlation coef	0.62	0.8	0.81
Sample size	6449	21 375	2589

For the Arctic, the overall speed RMS for these periods is 5.40 m s^{-1}, which is slightly lower than the 6 m s^{-1} RMS difference of the AVHRR cloud-drift winds determined by Herman (1993). In addition, the distribution of speed differences is nearly Gaussian, with the AVHRR winds having a noticeably slower speed bias when the difference is below 6 m s^{-1} and a faster speed bias associated with larger speed difference outliers (Fig. 5). The overall speed bias over the periods was found to be a minuscule −0.10 m s^{-1}, indicating that, on average, the AVHRR winds are slightly slower than the raob winds. This product would therefore help to reduce any long-term positive speed biases in the reanalysis winds. A strong correlation coefficient of about 0.8 is an additional indicator that the AVHRR winds over the Arctic are of good quality overall. Furthermore, the direction bias is under 0.5° counterclockwise (−0.45°) and the direction RMS is 54.76°. As is seen in Fig. 5, the distribution of direction differences is nearly Gaussian, with maximum frequency of direction difference near 0°.

To gain a better understanding of how AVHRR winds compare to the radiosonde winds, layer statistics were computed (Table 2; Fig. 6). Over the Arctic, it is obvious that, with increasing height in the atmosphere, the average absolute value and RMS speed differences increase. The speed RMS increases from 4.98 m s^{-1} at low levels to 7.57 m s^{-1} at upper levels. Schmetz et al. 1993 also observed an increase in speed RMS with height. The direction RMS and absolute-value differences decrease in quantity, or improve in quality, with

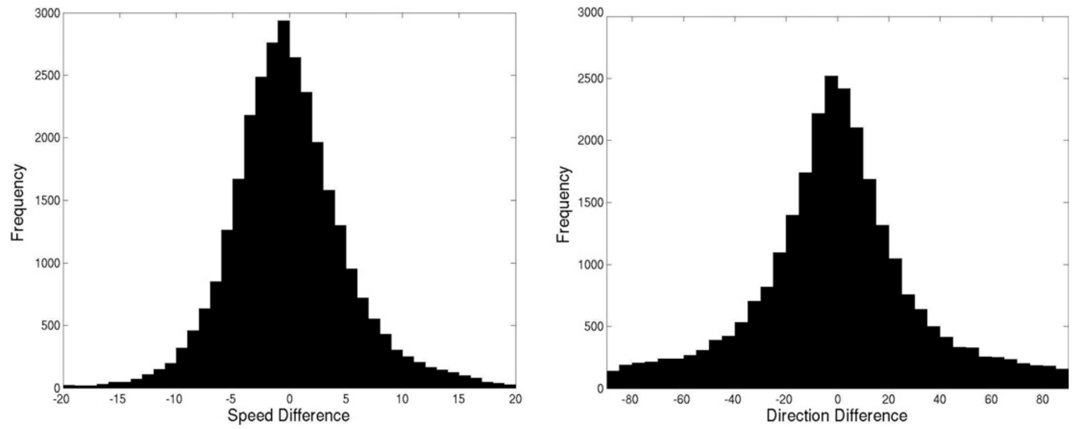

FIG. 5. Histograms of (left) speed and (right) direction differences of AVHRR winds relative to all raob winds over the Arctic within 100 km, 50 hPa, and 1 h of observation.

increased height, decreasing from 65.17° at low levels to 42.40° at upper levels. The direction bias is greatest at upper levels, at +1.48°, and is smallest at low levels, with direction bias of −0.49°. Overall, AVHRR is counterclockwise of the raob winds at low and middle levels and is more clockwise at upper levels. The speed biases are slightly positive (AVHRR +0.10 m s^{-1}) at low levels, negative at middle levels (AVHRR −0.29 m s^{-1}), and positive at upper levels (AVHRR +0.77 m s^{-1}). Table 2 shows that the NRMS (correlation coefficients) decrease (increase) from 0.68 (0.62) at low levels to 0.37 (0.81) at upper levels. This further demonstrates that the overall quality of the winds increases from low to upper levels.

It is important to compare the AVHRR and ERA-40 winds with rawinsondes that have not been assimilated into the reanalysis field. This will help to assess the quality of the AVHRR winds and will help to determine whether the AVHRR winds would be useful for assimilation into future reanalyses. The CEAREX and LeadEx field experiments were two cases in which the radiosonde wind data were not assimilated into the reanalysis products. Therefore, the wind data provided by these field experiments, which have been used in previous research to validate reanalysis winds (Francis 2002), are also used in this research project to determine the quality of AVHRR versus ERA-40 winds.

As is mentioned by Francis (2002) and indicated in Table 3, the ECMWF reanalysis has a significant positive speed bias in Arctic regions that are void of assimilated radiosonde data. Table 3 also indicates that AVHRR winds have a positive speed bias overall. However, the magnitude of the speed bias is 0.41 m s^{-1}, which is much smaller than the 1.64 m s^{-1} bias for ERA-40 (Fig. 7). The smaller speed bias of AVHRR was found to be significant at a 99% confidence level at low levels and at 90% overall with the use of the statistical *t* test. The slower speed difference of AVHRR versus ERA-40 at low levels is also seen in Table 4 and is a further indication that ERA-40 is too fast and that the AVHRR winds have a better speed quality at low levels. In addition, the AVHRR winds have smaller average absolute and RMS speed differences than those of ERA-40. However, it is also observed that ERA-40 has a smaller direction bias and RMS difference (Table 3). The direction bias is noticeably better in ERA-40 at low levels: +2.19° as compared with −9.61° for AVHRR (Table 3). At middle levels, AVHRR winds had a noticeably better direction bias of −0.09° as compared with −7.22° for ERA-40. The smaller speed bias and RMS difference of AVHRR over ERA-40 shows that AVHRR has potential to be assimilated into future ECMWF reanalysis products to correct for the positive speed bias. However, because of the paucity of independent and accurate wind observations that are not assimilated into the climate reanalysis, more independent data are needed to verify whether AVHRR has an overall more accurate wind field than ERA-40, especially at upper levels. Also, Francis (2002) shows that the same positive speed bias is in the NCEP–NCAR reanalysis over the Arctic. Therefore, AVHRR also has the potential to improve that reanalysis product.

5. Comparison with ERA-40

A comparison of AVHRR AMVs with the reanalysis winds will help to determine whether there are any biases in the reanalysis winds. It is important to deter-

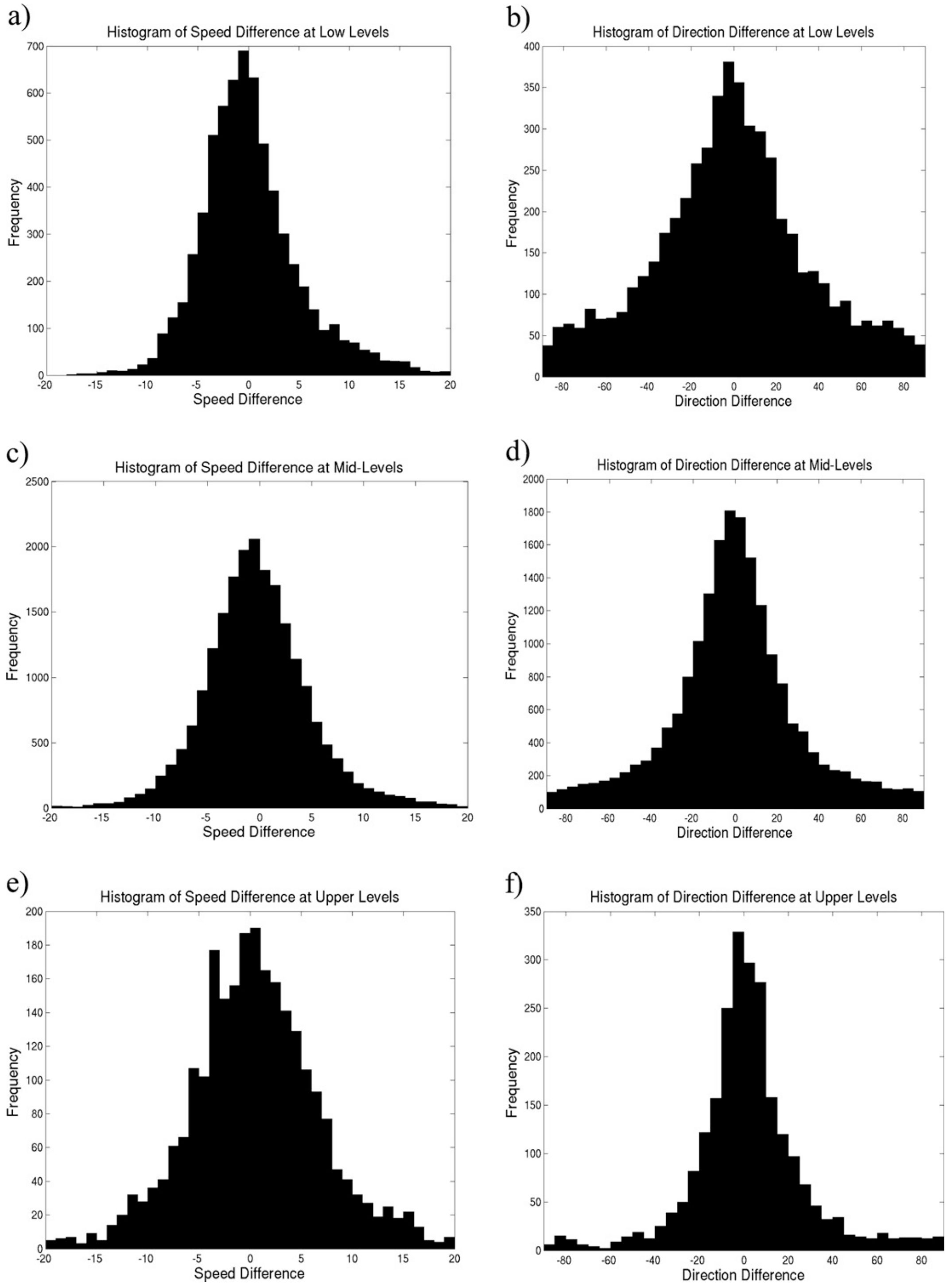

FIG. 6. Histograms of (left) speed and (right) direction differences between AVHRR and raob winds at (a), (b) low levels below (in height) 700 hPa; (c), (d) midlevels from 700 to 400 hPa, and (e), (f) upper levels above 400 hPa.

mine the atmospheric conditions that produce the greatest differences between both products. For example, are there atmospheric conditions under which the ERA-40 winds show a bias, or for which differences between the ERA-40 and AVHRR winds are large?

a. Long-term statistics

A long-term statistical comparison of AVHRR and ERA-40 winds (Table 4) over the Arctic for over 300 000 cases from 1992 through 2000 is given for three

TABLE 3. Statistical comparison of the AVHRR and radiosonde winds that are not assimilated into the reanalysis from CEAREX and LeadEx. Because of the sparsity of upper-level (above 400 hPa) collocations (within a point difference of 100 km by 50 hPa) of AVHRR with ERA-40, the layer statistics of mid- and upper levels are combined.

	Low levels (≤700 hPa)		Mid- and upper levels (>700 hPa)		Tot (all levels)	
	ERA-40	AVHRR	ERA-40	AVHRR	ERA-40	AVHRR
Speed RMS (m s^{-1})	5.85	5.68	7.74	7.61	6.69	6.55
Speed bias (m s^{-1})	+1.45	−0.19	+1.92	+1.28	+1.64	+0.41
Avg speed diff (m s^{-1})	4.06	3.77	5.08	5.16	4.47	4.34
Direction RMS (°)	52.02	53.20	53.83	58.01	52.79	55.21
Direction bias (°)	+2.19	−9.61	−7.22	−0.09	−1.66	−5.70
Mean speed (m s^{-1})	6.90	5.26	9.11	8.47	7.79	6.56
Mean raob speed (m s^{-1})	5.45		7.19		6.15	
Collocations	350		243		593	

layers in terms of the wind speed and direction RMS difference, the average difference, and the mean wind speeds. The statistical comparisons between AVHRR and ERA-40 indicate that the average speed difference changes sign from positive (AVHRR being faster than ERA-40) at upper levels to negative (AVHRR being slower than ERA-40) at lower levels. The speed RMS over the Arctic remains fairly constant over low and middle levels and then increases by 0.5 m s^{-1} at upper levels. The average direction differences are positive (AVHRR clockwise of ERA-40) for middle to upper levels and are negative (counterclockwise) at lower levels. The direction RMS decreases from lower to upper levels, with the greatest direction RMS difference of 17.66° at lower levels and smallest RMS difference of 11.54° at upper levels over the Arctic. The normalized speed RMS difference over the Arctic is 14% of the mean ERA-40 wind speed at upper levels and increases to 18% at middle levels and 24% at low levels. Overall, the AVHRR and ERA-40 winds agree fairly well. The difference distributions of speed and direction at low, middle, and high levels are nearly Gaussian, with maximum frequency of speed and direction differences occurring near zero.

b. *Kinematic flow type*

Speed and direction differences between AVHRR and ERA-40 were examined in terms of their location in the atmospheric flow (i.e., trough versus ridge or jet entrance versus exit) to determine whether there are any particular biases with respect to the atmospheric flow field. To determine the kinematic flow types, a geostrophic wind field was calculated with the use of the ERA-40 geopotential fields. A wind vector was determined to occur in a ridge (trough) if the relative vorticity was negative (positive). A wind vector was determined to be in a jet exit (entrance) if the gradient of the wind speed was less (greater) than −0.35 m s^{-1}

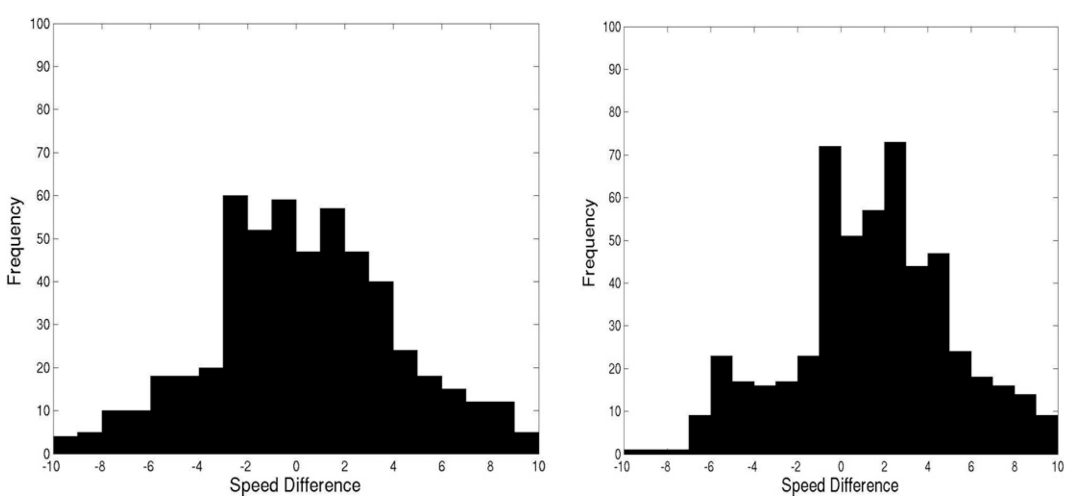

FIG. 7. Histograms of speed differences of (left) AVHRR and (right) ERA-40 winds relative to LeadEx and CEAREX raob winds over the Arctic within 100 km, 50 hPa, and 1 h of observation.

TABLE 4. Statistics for AVHRR winds over the Arctic in comparison with ERA-40.

	Low level (<700 hPa)	Midlevels (700–400 hPa)	Upper levels (>400 hPa)
Speed RMS (m s^{-1})	2.94	2.93	3.45
Speed diff (m s^{-1})	−0.32	−0.11	0.34
Direction RMS (°)	17.66	14.16	11.54
Direction diff (°)	−0.47	0.13	0.51
Mean AVHRR speed (m s^{-1})	12.35	15.91	25.36
Mean ERA-40 speed (m s^{-1})	12.67	16.02	25.02
Sample size	48 382	224 952	27 741

km^{-1} (+0.35 m s^{-1} km^{-1}) and in a jet streak when the AVHRR wind speed was equal to or greater than 25 m s^{-1}. Moreover, speed and direction differences were compared among quadrants of the jet streak. A wind vector was determined to be in the left (right) jet exit if the gradient was below the given threshold (−0.35 m s^{-1} km^{-1}) and the sign of vorticity advection was positive (negative):

$$\mathbf{V}\cdot\nabla(\zeta+f_0)=\mathbf{V}\cdot\nabla[(\partial V/\partial x-\partial U/\partial y)+f_0], \quad (3)$$

where $\mathbf{V}$ is the total wind, ζ is vorticity, x and y are Cartesian coordinates, U (V) is the east–west (north–south) wind component, and f_0 is the Coriolis parameter. A wind vector was determined to be in the left (right) jet entrance region when the gradient was above the given threshold (+0.35 m s^{-1} km^{-1}) and the sign of vorticity advection was negative (positive).

At upper (above 500 hPa) and middle levels (700–500 hPa), the AVHRR wind speed was slower than ERA-40 in troughs and faster than ERA-40 in ridges. However, the differences were not significant and were, on average, small in magnitude (Table 5). The distribution of the speed and direction differences in troughs and ridges was close to Gaussian (not shown). However, if ridges (troughs) are defined by a relative vorticity less than -4×10^{-5} s^{-1} (greater than 4×10^{-5} s^{-1}), rather than simply less than (greater than) 0, the magnitude of the differences increases for the most part, especially in midlevel troughs (Table 5). Above 500 hPa in ridges, the frequency of speed differences greater than 3 m s^{-1} that are faster (positive) is 54%, and the frequency of slower (negative) large differences is 46% (Fig. 8). In troughs, the percentages are the same but are reversed in sign, with 54% of the larger differences being slower (negative) and 46% being faster (positive). The sign of the difference is what is expected if the magnitude of the ageostrophic wind is underestimated because of centripetal acceleration around the base of the ridge or the trough (Fig. 9):

$$V_{\mathrm{gr}}=\left(1+KV_{\mathrm{gr}}/f_0\right)^{-1}V_g \quad \text{and} \quad (4)$$

$$V_a=V_{\mathrm{gr}}-V_g=-\left(KV_{\mathrm{gr}}/f_0\right)V_{\mathrm{gr}}, \quad (5)$$

where V_{gr} is the gradient wind, K is curvature, V_{g} is the geostrophic wind, V_a is the ageostrophic wind, and f_0 is the Coriolis parameter.

On the other hand, the small magnitude of the differences and their Gaussian distribution at upper levels indicate that even though there is a possible underestimation of the ageostrophic wind component in troughs and ridges by ERA-40, it is not a common trend in the reanalysis. However, at middle levels the average speed difference is 0.37 m s^{-1} slower in troughs, with the frequency of the slower large speed differences (greater than 3 m s^{-1}) being 62% and that for faster large speed differences being only 38% (Table 5). This indicates that an underestimation of the ageostrophic wind component in midlevel troughs in ERA-40 is more common during this case study (Fig. 10). However, in ridges at middle levels, the average speed difference is an insignificant −0.05 m s^{-1}.

Also notable is that, on average, AVHRR is faster and more counterclockwise in direction than ERA-40 in the jet entrance regions and is slower and more clockwise in direction in the jet exit regions at upper levels (Table 6). The average speed difference is −0.13 m s^{-1} and the direction difference is +0.53° in the jet exit region, with an average +0.17 m s^{-1} speed difference and −0.54° direction difference in the jet entrance

TABLE 5. Statistical comparison of AVHRR and ERA-40 winds between regions of positive ($\xi > 0$) and negative ($\xi < 0$) vorticity and between regions of stronger positive ($\xi > +4\times10^{-4}$) and negative ($\xi < -4\times10^{-4}$) vorticity.

	Midlevels (700–500 hPa)			Upper levels (above 500 hPa)		
	Avg (m s^{-1})	>+3 m s^{-1}	<−3 m s^{-1}	Avg (m s^{-1})	>+3 m s^{-1}	<−3 m s^{-1}
$\xi > 0$	−0.07	47%	53%	−0.06	46%	54%
$\xi < 0$	+0.06	51%	49%	+0.11	49%	51%
$\xi > +4\times10^{-4}$	−0.37	38%	62%	−0.12	46%	54%
$\xi < -4\times10^{-4}$	−0.05	47%	53%	+0.13	54%	46%

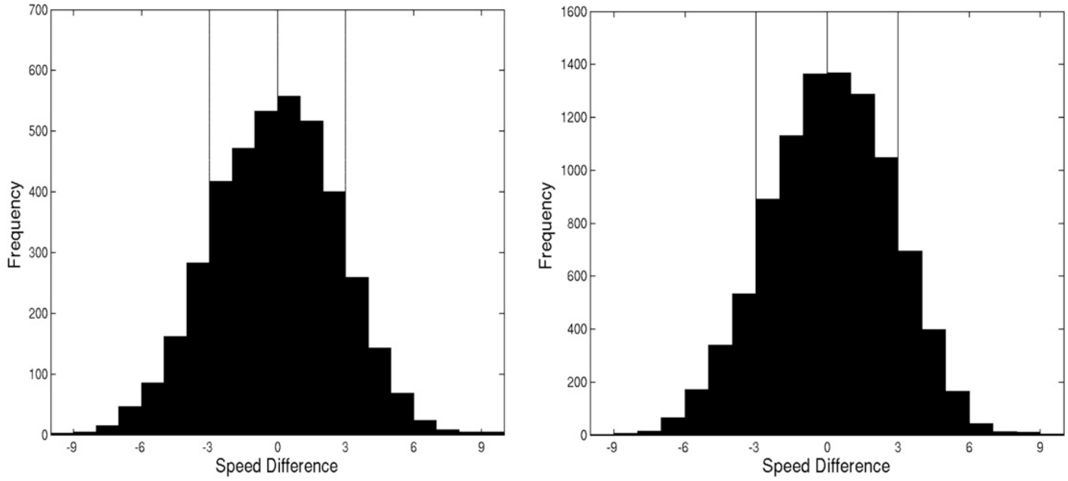

FIG. 8. Histograms of speed differences (AVHRR minus ERA-40) at upper levels (above 500 hPa) in (left) troughs or cyclones (relative vorticity greater than $+4 \times 10^{-5}$ s^{-1}) and (right) ridges or anticyclones (relative vorticity less than -4×10^{-5} s^{-1}).

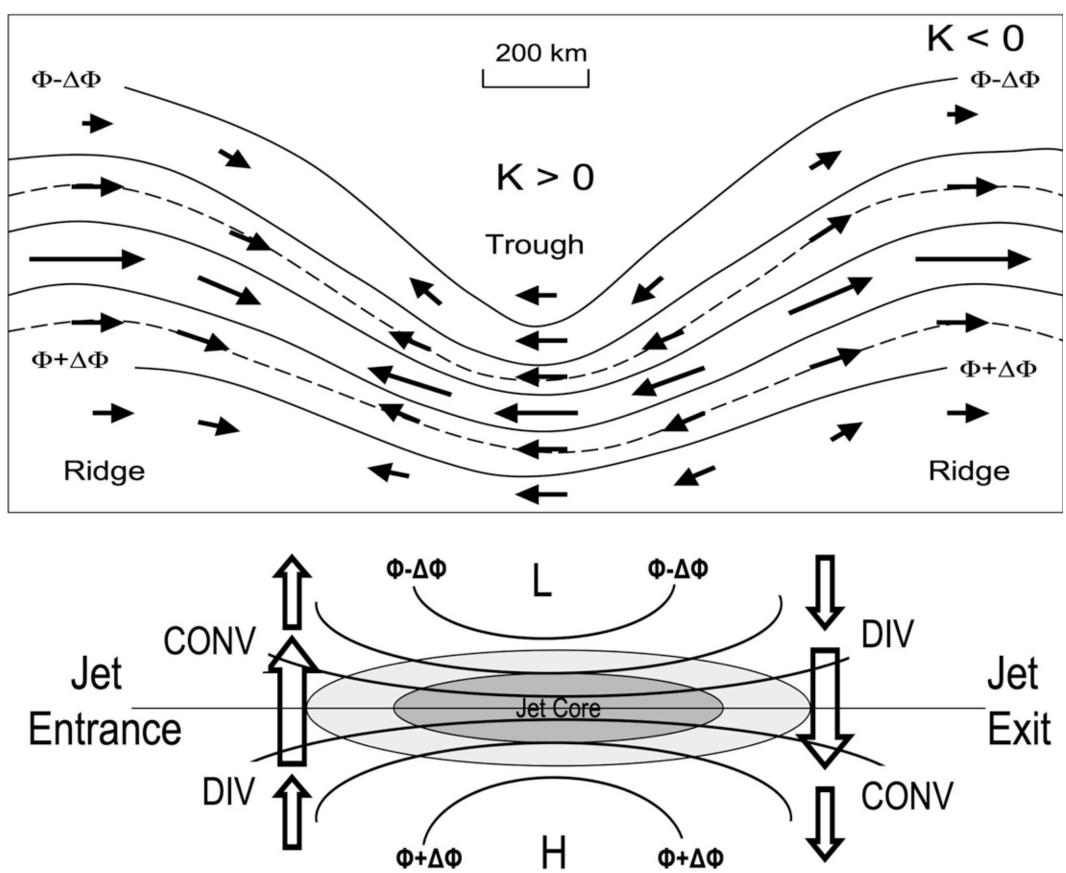

FIG. 9. (top) A typical flow pattern of the ageostrophic wind (black arrows) parallel to the geopotential height lines (black lines) in a curved westerly jet embedded in a highly amplified atmospheric wave. (bottom) A typical ageostrophic flow with the divergence and convergence patterns associated with the jet entrance and exit regions.

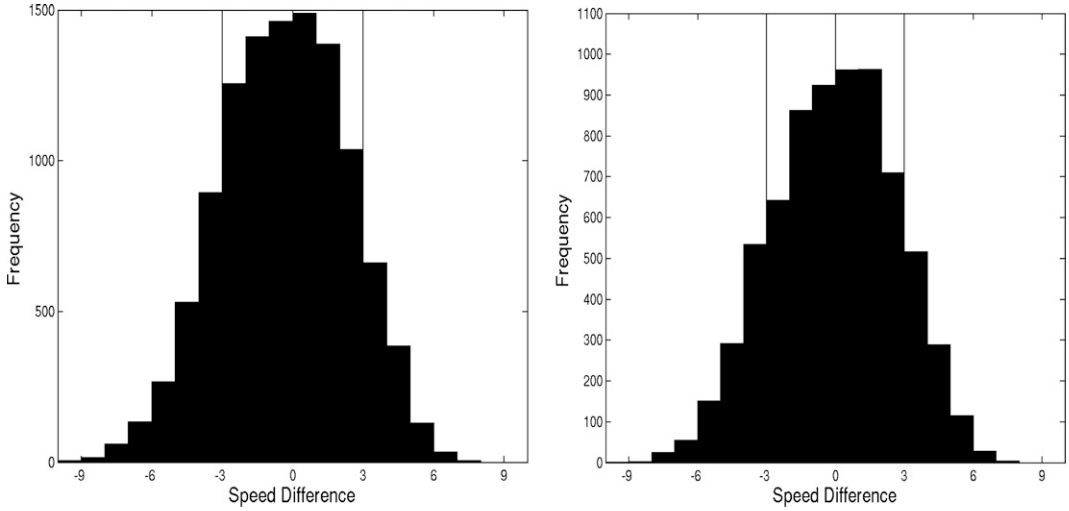

FIG. 10. As in Fig. 8, but at midlevels (500–700 hPa).

region. In contrast, outside the jet exit or jet entrance regions at upper levels, the average speed and direction differences are only $+0.09$ m s^{-1} and 0°, respectively. More significant is the average speed difference in the jet entrance region, and direction and speed differences in the jet exit region at middle levels (Table 6). The average direction difference is $+1.06°$ in the jet exit region and $-0.29°$ in the jet entrance region, and the average speed difference is -0.44 m s^{-1} in the jet entrance region and -0.60 m s^{-1} in the jet exit region. For all other wind vectors at middle levels during the case period, the average speed and direction differences are only $+0.02$ m s^{-1} and $+0.18°$, respectively. Most significant is the larger frequency of slower speed differences (<-3 m s^{-1}) of AVHRR winds relative to ERA-40 in the jet entrance and exit regions (Fig. 11; Table 6).

For midlevel cases with an absolute magnitude of the wind speed difference greater than 3 m s^{-1} in the jet entrance region, 71% of the time the AVHRR winds were slower than ERA-40. In the jet exit region, 76% of the time the AVHRR winds were slower than the ERA-40 winds. For cases with direction differences greater than 15°, 63% of the time the sign was positive (clockwise) in the jet exit regions at midlevels. Overall, AVHRR wind vectors in the jet exit regions, especially at midlevels, have a more rapid deceleration of the wind coming out of the jet. The AVHRR winds have a slower acceleration into the jet entrance region at midlevels. Less significant, but of note, is the faster acceleration of the wind speed in the jet entrance region and the greater deceleration of the wind speed in the jet exit region at upper levels. The AVHRR wind vectors are clockwise of the ERA-40 wind vector in the jet exit region, on average, especially at midlevels, and are counterclockwise of the ERA-40 wind vector in the jet entrance region at middle and upper levels. The more clockwise wind direction observed for AVHRR in the jet exit region at midlevels is a possible underestimation of the cross-isoheight ageostrophic flow in the jet exit region by ERA-40 (Fig. 9).

Last, when separating cases in which the AVHRR wind speed was equal to or greater than 25 m s^{-1} (jet speeds) from those in which it was less than 25 m s^{-1}, a noticeable speed difference bias was observed. For

TABLE 6. Statistical comparison of AVHRR and ERA-40 winds in jet exit and jet entrance regions.

	Midlevels (700–500 hPa) jet entrance	Midlevels (700–500 hPa) jet exit	Upper levels (above 500 hPa) jet entrance	Upper levels (above 500 hPa) jet exit
Avg speed diff (m s^{-1})	-0.44	-0.60	$+0.17$	-0.13
Avg direction diff (°)	-0.29	$+1.06$	-0.54	$+0.53$
$>+3$ m s^{-1}	29%	24%	54%	42%
<-3 m s^{-1}	71%	76%	46%	58%
$>+15°$	42%	63%	45%	59%
$<-15°$	58%	37%	55%	41%

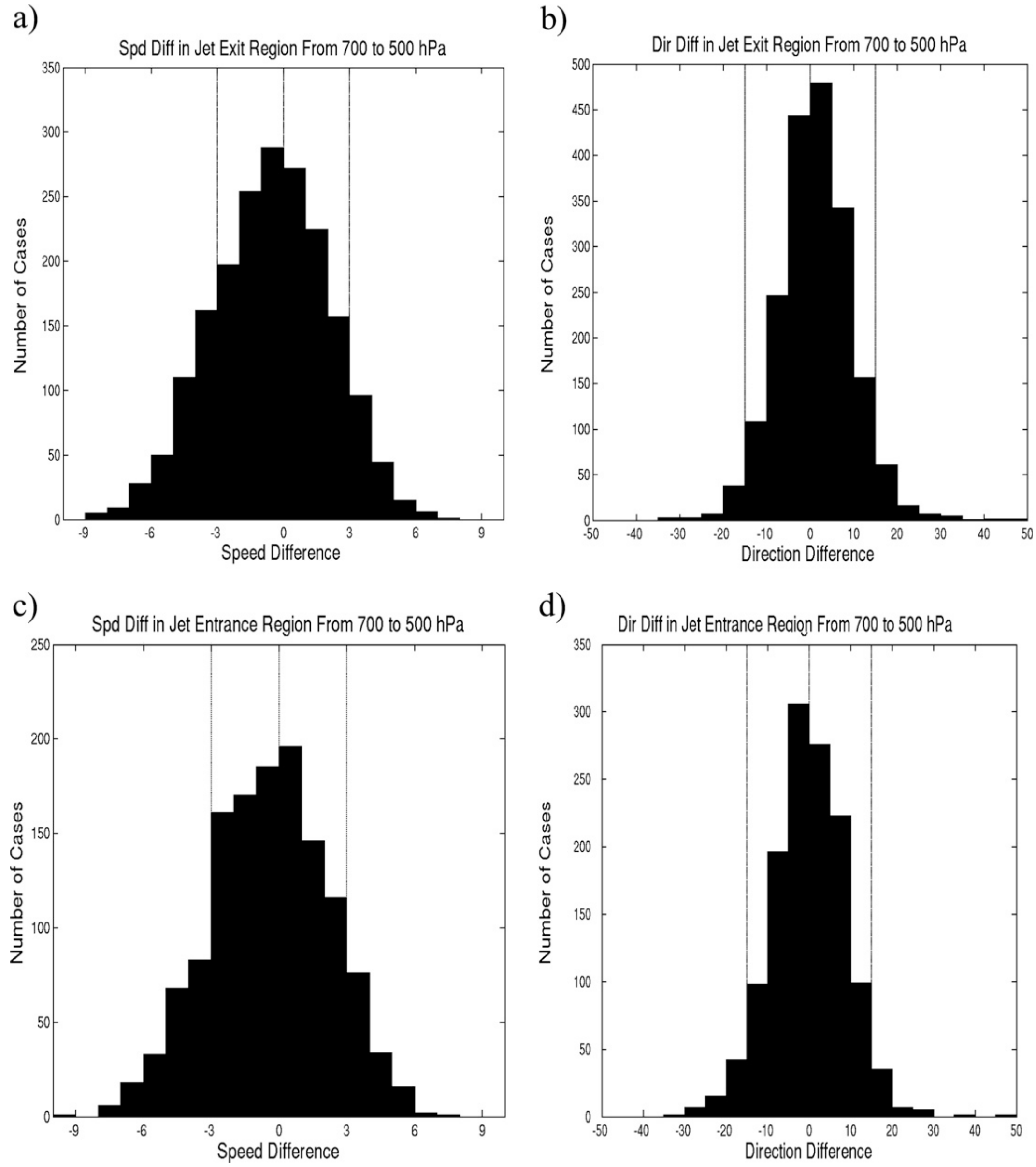

FIG. 11. Histograms of differences (AVHRR minus ERA-40) at midlevels (700–500 hPa) for (a) speed and (b) direction (positive: clockwise of the ERA-40 wind vector; negative: counterclockwise of the ERA-40 wind vector) at jet exit region, defined as less than -0.35 m s^{-1} km^{-1} wind speed gradient along the isoheight. (c), (d) As in (a) and (b), respectively, but at jet entrance region, defined as greater than $+0.35$ m s^{-1} km^{-1} wind speed gradient along the isoheight.

AVHRR wind speeds greater than or equal to 25 m s^{-1} that typically occur in jet streaks, AVHRR winds were noticeably faster than ERA-40 winds (Fig. 12; Table 7). At upper levels, 70% of the speed differences greater than 3 m s^{-1} were positive (AVHRR faster than ERA-40) and only 30% of the speed differences greater than 3 m s^{-1} were slower than ERA-40. For speeds less than 25 m s^{-1}, AVHRR was on average slower than ERA-40, with larger speed differences (greater than 3 m s^{-1}) being 57% negative. Overall, the slower speed tendency of the AVHRR winds in lower wind speed conditions is not as significant as the higher-speed tendency seen in the AVHRR jet speeds. In AVHRR jet speeds at midlevels, the average difference was noticeably positive, with 81% of the speed differences greater than 3 m s^{-1} being faster. Also, at middle levels, it was found that AVHRR was slightly slower in wind speeds less than 25 m s^{-1}. Especially noticeable at middle levels is

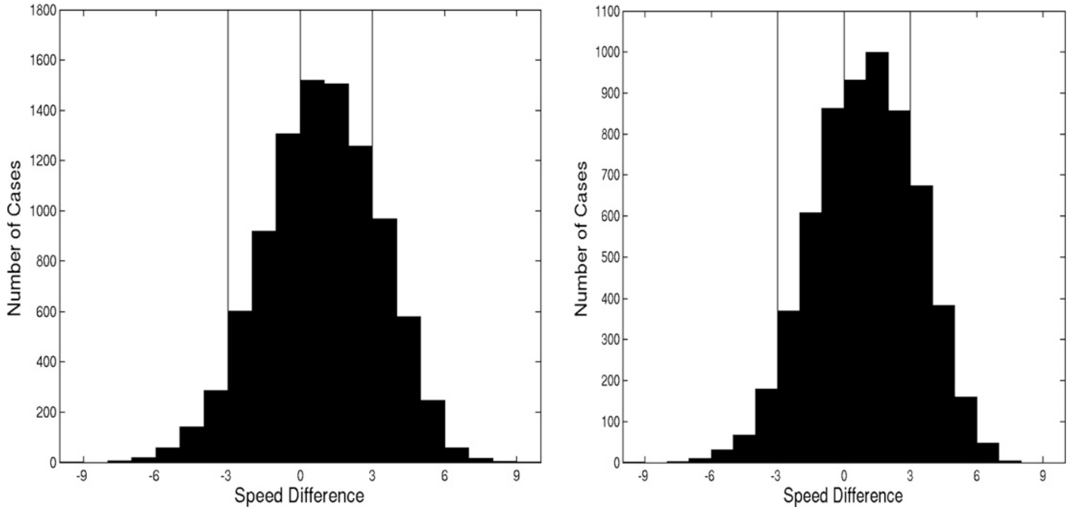

FIG. 12. Histograms of speed differences (AVHRR minus ERA-40) for AVHRR wind speeds $\geq$25 m s^{-1} at (left) upper levels (above 500 hPa) and (right) midlevels (700–500 hPa).

that the slower speed tendency of AVHRR in the slower wind speed condition (less than 25 m s^{-1}) is not as significant as the faster speed tendency seen in stronger winds. Overall, the noticeable faster speed difference of AVHRR relative to ERA-40 in wind speeds greater than 25 m s^{-1} is an indication that ERA-40 either is underestimating wind speeds in jets or is misplacing the location of jet streaks, or it is a product of incorrect height assignments of the AVHRR winds.

6. Summary and conclusions

The ability to track atmospheric motions using satellite imagery has led to the production of a 20-yr dataset of winds over the polar regions using the AVHRR instrument on NOAA polar-orbiting satellites. The AVHRR winds were developed by calculating the displacement of individual cloud features in the 11-μm infrared channel. Vigorous postprocessing eliminates potentially bad wind vectors by checking the consistency of the satellite-derived wind vectors in time and space and in comparison with the background wind field. The development of the wind product was motivated by observed errors in ECMWF and NCEP–NCAR reanalysis products (Francis 2002). Errors in the wind field could cause semipermanent and fluctuating synoptic-scale features in the reanalysis field to be misplaced, and synoptic-scale ageostrophic motions in the wind field could be underestimated.

Validation of AVHRR and ERA-40 winds relative to rawinsondes from LeadEx (1992) and CEAREX (1988–89) that were not assimilated into the reanalysis indicated that AVHRR had a smaller speed bias by over 1 m s^{-1} and had a smaller RMS by 0.14 m s^{-1} but had a larger direction bias and RMS difference. With the majority (99%) of the collocations coming below 400 hPa, it is an indication that AVHRR has higher quality in wind speed but a somewhat lower quality in wind direction at those experimental sites at low–midlevels, on average.

Comparisons of AVHRR winds with raobs show that the quality of the winds over the Arctic is high, with the largest differences below 700 hPa and the smallest above 400 hPa, because the direction quality of the wind vector improves with height. On the other hand, the speed RMS increases from lower to upper levels. Moreover, the NRMS errors (correlation coefficients) of the wind vectors decrease (increase) with height, in-

TABLE 7. Statistical comparison of AVHRR and ERA-40 wind speed when AVHRR wind speeds are at least 25 m s^{-1} vs when AVHRR wind speeds are less than 25 m s^{-1}.

	Midlevels in jet speed $\geq$25 m s^{-1}	Midlevels not in jet speed <25 m s^{-1}	Upper levels in jet speed $\geq$25 m s^{-1}	Upper levels not in jet speed <25 m s^{-1}
Avg speed diff (m s^{-1})	+0.95	−0.08	+0.65	−0.20
>+3 m s^{-1}	81%	47%	70%	43%
<−3 m s^{-1}	19%	53%	30%	57%

dicating that the overall quality of the wind vectors increases with height.

AVHRR and ERA-40 wind fields are, on average, similar, with direction RMS values of less than 20° and speed RMS values of less than 4 m s^{-1}. On average, AVHRR is slower and more counterclockwise in direction at low levels (below 700 hPa) and is faster and more clockwise at upper levels (above 500 hPa).

When comparing regions of positive vorticity (troughs and cyclones) with regions of negative vorticity (ridges and anticyclones), it was found that AVHRR winds were, on average, slower in regions of positive vorticity and faster in regions of negative vorticity. This was found to be more noticeable when the relative vorticity threshold was increased to $\pm 4 \times 10^{-5}$ s^{-1}. However, with the slight exception of the slow bias of -0.37 m s^{-1} in midlevel troughs, this is not found to be distinct. Furthermore, the obvious negative speed bias in troughs at middle levels could be an indication of underestimation by ERA-40 of the ageostrophic flow that opposes the geostrophic flow in troughs, slowing down the overall wind speed in flow in and around troughs.

In addition, AVHRR-derived winds are noticeably slower and more clockwise in the jet exit regions and slower in entrance regions at midlevels (700–500 hPa). This could result from ERA-40 underestimating the deceleration of the wind speed coming out of the jet streak, overestimating the acceleration of the wind speed coming into the jet at middle levels, and possibly underestimating the ageostrophic flow across the isoheights in the midlevel jet exit regions especially. At upper levels (above 500 hPa), although not as significant as was seen at midlevels, the AVHRR wind vectors on average are slower and more clockwise of the ERA-40 wind vectors in the jet exit and are observed to be faster and counterclockwise of the ERA-40 wind vectors in the jet entrance region. This shows slight underestimation of the acceleration of the wind into the jet streak and deceleration of the wind out of the jet streak and possible underestimation of the ageostrophic flow across the isoheights of the jet exit and entrance regions. However, excluding the underestimation of the deceleration of wind speed and cross-isoheight flow coming out of the jet exit at middle levels, the biases in speed and direction are found to be relatively small.

Furthermore, AVHRR is noticeably faster than ERA-40 at wind speeds greater than or equal to 25 m s^{-1} (jet streaks) with larger faster differences (greater than 3 m s^{-1}) being 40% more frequent at upper levels and 62% more frequent at midlevels. This is a strong indication that AVHRR has stronger winds in jet streams overall. This could be a result either of ERA-40 misplacing the location of the jet streak or of the satellite wind height assignment method consistently assigning pressure heights of the wind vectors of optically thin clouds too low in altitude. Further investigation is needed on this issue.

Acknowledgments. This research was supported by the NOAA/NESDIS Center for Satellite Applications and Research and by the NASA Science Mission Directorate. We thank Dave Santek for technical help and many useful discussions and Steve Ackerman and Chris Velden for suggestions. Jon Martin was an endless source of ideas on kinematics. Eli Hunter and Jennifer Francis at Rutgers University and Ola Persson at the University of Colorado provided LeadEx and CEAREX data. The ECMWF reanalysis data were obtained from the ERA-40 project Web site. AVHRR data were obtained from the NOAA CLASS archive system. Dan Baldwin at the University of Colorado provided the software for navigation and calibration of the AVHRR data. The views, opinions, and findings contained in this report are those of the authors and should not be construed as an official National Oceanic and Atmospheric Administration or U.S. government position, policy, or decision.

REFERENCES

Comiso, J. C., 2002: A rapidly declining perennial sea ice cover in the Arctic. *Geophys. Res. Lett.,* **29,** 1956, doi:10.1029/2002GL015650.

——, 2003: Warming trends in the Arctic from clear sky satellite observations. *J. Climate,* **16,** 3498–3510.

Dure, I., R. S. Vose, and D. B. Wuertz, 2006: Overview of the integrated global radiosonde archive. *J. Climate,* **19,** 53–68.

Francis, J. A., 2002: Validation of reanalysis upper-level winds in the Arctic with independent rawinsonde data. *Geophys. Res. Lett.,* **29,** 1315, doi:10.1029/2001GL014578.

——, E. Hunter, and C. Z. Zou, 2005: Arctic tropospheric winds derived from TOVS satellite retrievals. *J. Climate,* **18,** 2270–2285.

Fyfe, J. C., 2003: Extratropical Southern Hemisphere cyclones: Harbingers of climate change? *J. Climate,* **16,** 2802–2805.

Haimberger, L., 2005: Homogenization of radiosonde temperature time series using ERA-40 analysis feedback information. ECMWF ERA-40 Project Rep. Series 20, 75 pp.

Hayden, C. M., and R. J. Purser, 1995: Recursive filter objective analysis of meteorological fields: Applications to NESDIS operational processing. *J. Appl. Meteor.,* **34,** 3–15.

Herman, L. D., 1993: High frequency satellite cloud motion at high latitudes. Preprints, *Eighth Symp. on Meteorological Observations and Instrumentation*, Anaheim, CA, Amer. Meteor. Soc., 465–468.

Holland, M. M., 2003: The North Atlantic Oscillation–Arctic Oscillation in the CCSM2 and its influence on Arctic climate variability. *J. Climate,* **16,** 2767–2781.

Holmlund, K., 1998: The utilization of statistical properties of satellite-derived atmospheric motion vectors to derive quality indicators. *Wea. Forecasting,* **13,** 1093–1104.

——, C. S. Velden, and M. Rohn, 2001: Enhanced automated quality control applied to high-density satellite winds. *Mon. Wea. Rev.,* **129,** 517–529.

Jacobs, S. S., and J. C. Comiso, 1997: Climate variability in the Amundsen and Bellinghausen Seas. *J. Climate,* **10,** 697–709.

Key, J. R., and A. C. K. Chan, 1999: Multidecadal global and regional trends in 1000 mb and 500 mb cyclone frequencies. *Geophys. Res. Lett.,* **26,** 2053–2056.

——, D. Santek, C. S. Velden, N. Bormann, J. Thepaut, L. P. Riishojgaard, Y. Zhu, and W. P. Menzel, 2003: Cloud-drift and water vapor winds in the polar regions from MODIS. *IEEE Trans. Geosci. Remote Sens.,* **41,** 482–492.

Kitchen, M., 1989: Representativeness errors for radiosonde observations. *Quart. J. Roy. Meteor. Soc.,* **115,** 673–700.

Lindsay, R. W., and J. Zhang, 2005: The thinning of Arctic sea ice, 1988–2003: Have we passed a tipping point? *J. Climate,* **18,** 4879–4894.

Liu, Y., and J. R. Key, 2003: Detection and analysis of clear-sky, low-level atmospheric temperature inversions with MODIS. *J. Atmos. Oceanic Technol.,* **20,** 1727–1737.

——, ——, A. Schweigler, and J. Francis, 2006: Characteristics of satellite-derived clear sky atmospheric temperature inversion strength in the Arctic, 1980–96. *J. Climate,* **19,** 4902–4913.

Nieman, S. J., W. P. Menzel, C. M. Hayden, D. Gray, S. T. Wanzong, C. S. Velden, and J. Daniels, 1997: Fully automated cloud-drift winds in NESDIS operations. *Bull. Amer. Meteor. Soc.,* **78,** 1121–1133.

Polyakov, I. V., R. V. Bekryaev, G. V. Alekseev, and U. S. Bhatt, 2003: Variability and trends of air temperature and pressure in the maritime Arctic, 1875–2000. *J. Climate,* **16,** 2067–2077.

Schmetz, J., K. Holmlund, J. Hoffman, B. Strauss, B. Mason, V. Geartner, A. Koch, and L. Van De Berg, 1993: Operational cloud-motion winds from Meteosat infrared images. *J. Appl. Meteor.,* **32,** 1206–1225.

Serreze, M. C., and Coauthors, 2000: Observational evidence of recent change in the northern high-latitude environment. *Climatic Change,* **46,** 159–207.

Shapiro, M. A., and P. J. Kennedy, 1981: Research aircraft measurements of jet stream geostrophic and ageostrophic winds. *J. Atmos. Sci.,* **38,** 2642–2652.

Thompson, D. W. J., and S. Solomon, 2002: Interpretation of recent Southern Hemisphere climate change. *Science,* **296,** 895–899.

Turner, J., and D. E. Warren, 1989: Cloud track winds in the polar regions from sequences of AVHRR images. *Int. J. Remote Sens.,* **10,** 695–703.

——, T. A. Lachlan-Cope, S. Colwell, G. J. Marshall, and W. M. Connolley, 2006: Significant warming of the Antarctic winter troposphere. *Science,* **311,** 1914–1917.

Uppala, S. M., and Coauthors, 2005: The ERA-40 reanalysis. *Quart. J. Roy. Meteor. Soc.,* **131,** 2961–3012.

Velden, C. S., C. M. Hayden, S. J. Nieman, W. P. Menzel, S. Wanzong, and J. S. Goerss, 1997: Upper-tropospheric winds derived from geostationary satellite water vapor observations. *Bull. Amer. Meteor. Soc.,* **78,** 173–195.

——, and Coauthors, 2005: Recent innovations in deriving tropospheric winds from meteorological satellites. *Bull. Amer. Meteor. Soc.,* **86,** 205–223.

Wang, X., and J. R. Key, 2005a: Arctic surface, cloud, and radiation properties based on the AVHRR Polar Pathfinder dataset. Part I: Spatial and temporal characteristics. *J. Climate,* **18,** 2558–2574.

——, and ——, 2005b: Arctic surface, cloud, and radiation properties based on the AVHRR Polar Pathfinder dataset. Part II: Recent trends. *J. Climate,* **18,** 2575–2593.

Zhang, X., J. E. Walsh, J. Zhang, U. S. Bhatt, and M. Ikeda, 2004: Climatology and interannual variability of Arctic cyclone activity: 1948–2002. *J. Climate,* **17,** 2300–2317.

Zou, C. Z., and M. L. Van Woert, 2001: The role of conservation of mass in the satellite-derived poleward moisture transport over the Southern Ocean. *J. Climate,* **14,** 997–1015.

——, and ——, 2002: Atmospheric wind retrievals from satellite soundings over the middle- and high-latitude oceans. *Mon. Wea. Rev.,* **130,** 1771–1791.